Available online at www.sciencedirect.com
ScienceDirect
Journal of Sound and Vibration 301 (2007) 207–225
JOURNAL OF SOUND AND VIBRATION
www.elsevier.com/locate/jsvi

Dynamic consequences of electromagnetic pull due to deviations in generator shape

Niklas L.P. Lundström*, Jan-Olov Aidanpää

Division of Computer Aided Design, Department of Applied Physics and Mechanical Engineering, Luleå University of Technology, SE-971 87, Sweden

Received 24 October 2005; received in revised form 8 September 2006; accepted 26 September 2006
Available online 6 December 2006

Abstract

Results from earlier measurements on hydropower generators have indicated relatively large eccentricities and shape deviations in the rotor and stator. These non-symmetric geometries produce an attraction force between the rotor and the stator, called unbalanced magnetic pull (UMP). The UMP force can produce large vibrations which can be dangerous to the machine. A mathematical model is developed to describe the shapes of the rotor and stator, and the corresponding UMP is obtained through the law of energy conservation. The target of the paper is to analyse the dynamics of a generator due to shape deviations in the rotor and stator. As rotor-model, a balanced Jeffcott rotor is used. A linearization of the UMP indicates the importance of considering the nonlinear effects. The stability of some attractors are analysed and the generator dynamics are further investigated by simulating the basin of attraction. The magnitudes are approximately obtained when the shape deviations become dangerous for the generator. It is concluded which shape deviations that are more dangerous than others. In hydropower generator maintenance the shapes of the rotor and stator are frequently measured. The results from this paper can be used to evaluate such measurements and estimate the stability and robustness by simulations.

1. Introduction

Hydropower generators have small air-gaps between the rotor and the stator. Usually, it is about 0.2% of the stator radius. Measurements on hydropower generator shapes are frequently carried out during maintenance, indicating that all hydropower generators are associated with some degree of asymmetry in the air-gap. Talas and Toom [1] have reported on a variation of the air-gap deviating more than ±10%. These asymmetries distort the air-gap flux density distribution, producing an attraction force between the rotor and the stator, called unbalanced magnetic pull (UMP). The effect of UMP can be vibrations which are dangerous to the machine. There are documented cases, e.g. Talas and Toom [1], where the rotor has been in contact with the stator due to air-gap asymmetry.

*Corresponding author.
E-mail addresses: niklas.lundstrom@math.umu.se (N.L.P. Lundström), joa@ltu.se (J.-O. Aidanpää).

0022-460X/$ - see front matter © 2006 Elsevier Ltd. All rights reserved.
doi:10.1016/j.jsv.2006.09.030

A literature survey indicates intensive study on the methods of calculating UMP caused by eccentricity, as well as the vibration characteristics of a rotor system due to UMP. Early papers, such as Behrend [2] and Robinson [3], suggested linear equations to calculate the magnetic pull for an eccentricity up to 10% of the average air-gap. Covo [4] and Ohishi et al. [5] improved the equations for calculating the magnetic pull by considering the effect of saturation on the magnetization curve. Belmans et al. [6] developed an analytic model for vibrations in induction motors. They showed that the UMP acting on the rotor also consisted of harmonic components. The paper put forward the idea of modulating the magnetic flux density by the air-gap permanence, expressed as a Fourier series. Fruchtenicht et al. [7] studied the self-excited transverse vibration of a four-pole machine, Belmans et al. [8] investigated the radial stability of the shaft in a two-pole machine whereas Smith and Dorrell [9] studied the UMP by winding analysis. Finite element analysis technique can now provide solutions of the UMP, though this approach is still very computationally expensive and can often not provide insight into the origins and key factors of its production, Debortoli et al. [10], Arkkio [11]. Dorrell [12] calculated UMP for non-uniform rotor eccentricity and tooth saturation, Guo et al. [13] studied the effects of UMP and the vibration level in three-phase generators with any number of pole pairs, Wang et al. [14] derived the UMP due to eccentricity through the law of energy conservation and studied the free and forced vibrations for rotors of electric motors, and Holopainen et al. [15] studied the rotordynamic effects of electromechanical interaction on induction motors. Karlsson and Aidanpää [16] studied the dynamic behaviour in a hydropower rotor system due to the influence of generator shape and fluid dynamics. Williamson and Abdel-Magied [17] calculated the UMP in induction motors with asymmetrical rotor cage. They showed that with an even distribution pattern of bar faults the UMP may be vanishingly small.

In this paper, the UMP due to an arbitrary disturbed air-gap is derived through the law of energy conservation. It is also compared to a linear model for calculating UMP. The dynamic consequences of UMP due to shape deviations on the rotor and stator are studied using a balanced Jeffcott rotor as a simplified model of a hydropower generator. A mathematical model describes the shapes of the rotor and stator. The dynamic behaviour of the generator is analysed through the use of symmetries for certain cases. For different shape deviations the basin of attraction is studied for rotor–stator impact motions. From this, the robustness of the generator is approximated for different rotor and stator shapes.

2. Generator geometry

Fig. 1 shows the geometry of the generator model, having an arbitrary non-circular shaped rotor and stator. The generator is treated as a balanced Jeffcott or Laval rotor having length l_0, mass γ and stiffness k of the generator axis. The rotor rotates at a constant counterclockwise angular speed ω. Point C_s gives the location of the bearings while point C_r is the rotational centre of the rotor. The coordinate system has the origin at C_s, r is the rotor radius and s is the stator radius.

Let r_0 and s_0 be the undisturbed radius of the rotor and the stator, respectively. An arbitrary non-circular shape can be described by adding a Fourier series of cosine terms to the rotor radius, r, and the

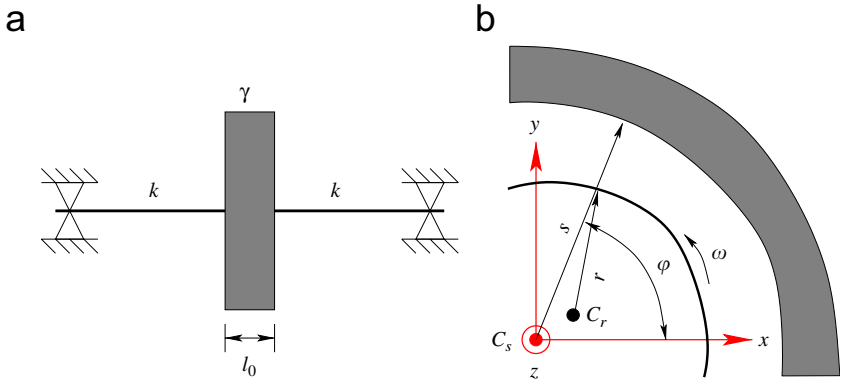

Fig. 1. The generator model; (a) the Jeffcott rotor; (b) the cross-section of the generator.

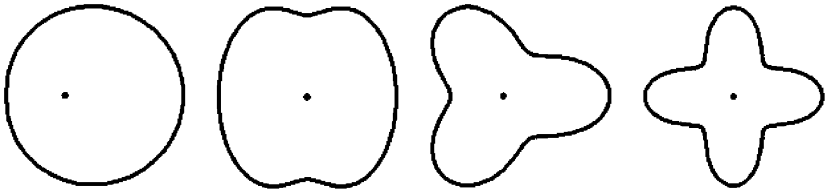

Fig. 2. The geometry of the rotor for $\delta_n^r = r_0/3, n = 1, 2, 3, 4$.

stator radius, s,

$$r = r_0(z) + \sum_{n=1}^{\infty} \delta_n^r(z) \cos n(\varphi + \alpha_n^r(z)), \tag{1}$$

$$s = s_0(z) + \sum_{m=1}^{\infty} \delta_m^s(z) \cos m(\varphi + \alpha_m^s(z)), \tag{2}$$

where

$$\delta_n^r(z) \geqslant 0, \quad \delta_m^s(z) \geqslant 0, \quad \sum_{n=1}^{\infty} \delta_n^r(z) + \sum_{m=1}^{\infty} \delta_m^s(z) < g_0(z). \tag{3}$$

Here, $g_0 = s_0 - r_0$ is the undisturbed air-gap, δ_n^r and δ_m^s are referred to as the rotor and stator perturbation parameters while α_n^r and α_m^s are the corresponding phase angles. To simplify notations, it is hereinafter assumed that $\delta_n^r = \delta_m^s = 0, \forall m, n \in \mathbf{N}$, if nothing else is mentioned. $\mathbf{N}$ is the set of all natural numbers. Fig. 2 shows the rotor geometry for $\delta_n^r = r_0/3$, $n = 1, 2, 3, 4$, and phase angle $\alpha_n^r = 0$. Note that the stator has the same geometry for $\delta_m^s = \delta_n^r$ and $m = n$.

The case $\delta_1^r > 0$ and $\delta_1^s > 0$ will correspond to rotor eccentricity and stator eccentricity, respectively. Since dynamic eccentricity is normally small compared to the dimensions of the generator, it is assumed that the perturbed air-gap (g) is

$$g = s(z, \varphi) - r(z, \varphi) - x \cos \varphi - y \sin \varphi, \tag{4}$$

where (x, y) gives the position of C_r. Eqs. (1), (2) and (4) gives, after adding the ω rotation

$$g = g_0(z) + \sum_{m=1}^{\infty} \delta_m^s(z) \cos m(\varphi + \alpha_m^s) - \sum_{n=1}^{\infty} \delta_n^r(z) \cos n(\varphi + \alpha_n^r(z) - \omega t) - x \cos \varphi - y \sin \varphi. \tag{5}$$

The geometric model is now completed.

3. Unbalanced magnetic pull

3.1. Calculation of the UMP

Based on the theory of magnetic field [18], the potential energy reserved in the air-gap can be expressed as

$$E = \int_{\text{all space}} \frac{B(x, y, z, t, \varphi)^2}{2\mu_0} \, \mathrm{d}V, \tag{6}$$

where B is the magnetic flux density (also called the B-field) in the air-gap and μ_0 is the permeability of air. For an approximation, the relations between the B-field and the air-gap widths are assumed as in Ref. [14],

$$B = \frac{B_0(z) g_0(z)}{g(x, y, z, t, \varphi)}. \tag{7}$$

B_0 is the uniformly distributed B-field for an undisturbed air-gap, i.e. $g = g_0$. Next, consider a volume element $\mathrm{d}V$ as shown in Fig. 3.

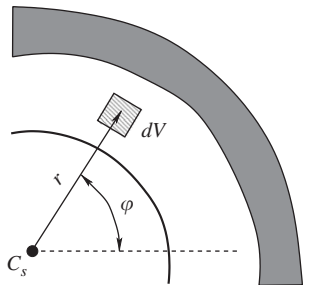

Fig. 3. The volume element $\mathrm{d}V$.

According to Eqs. (6) and (7), the potential energy, δE, reserved in $\mathrm{d}V$ is given as

$$\delta E = \frac{B_0(z)^2 g_0(z)^2}{2\mu_0 g(x,y,z,\varphi,t)^2}\,\mathrm{d}V. \tag{8}$$

Eq. (8) shows that if the air-gap is disturbed from the current value g to a new value $g+\mathrm{d}g$, δE will increase if $\mathrm{d}g<0$ and decrease if $\mathrm{d}g>0$. Let $\mathrm{d}E_{\mathrm{mech}}$ be increments of mechanical energy input to $\mathrm{d}V$ and $\mathrm{d}E_{\mathrm{electric}}$ increments of the electric energy output from $\mathrm{d}V$. When considering the energy conversion between the magnetic and mechanical fields over an infinitesimal period of time, the law of energy conservation requires, after neglecting losses

$$\mathrm{d}E_{\mathrm{mech}} = \mathrm{d}(\delta E) + \mathrm{d}E_{\mathrm{electric}}. \tag{9}$$

As in the case of eccentricity [14], it is assumed that the electric energy output from the generator is independent of the air-gap variations, thus $\mathrm{d}E_{\mathrm{electric}}=0$. If $\mathrm{d}g<0$, then $\mathrm{d}(\delta E)=\mathrm{d}E_{\mathrm{mech}}>0$. Since the mechanical energy input increases when g decreases, a force acting in the radial direction has to be present. This force is denoted by $\mathrm{d}f$. Then, the virtual work done by this force is $\mathrm{d}f\,\mathrm{d}g=-\mathrm{d}(\delta E)$, which gives

$$\mathrm{d}f = -\frac{\mathrm{d}}{\mathrm{d}g}(\delta E). \tag{10}$$

In Eq. (8), note that, since $\mathrm{d}V = r\,\mathrm{d}r\,\mathrm{d}z\,\mathrm{d}\varphi$, the potential energy δE will increase if r increases when g is constant. This small change in $\mathrm{d}f$ cannot be considered in Eq. (10). But, since the change of g and r is of approximately the same size and $g \ll r$, the change of δE due to variations in r is considered to be negligible. Therefore, to simplify the calculations it is assumed that $\mathrm{d}V = u_0\,\mathrm{d}r\,\mathrm{d}z\,\mathrm{d}\varphi$, where $u_0=(r_0+s_0)/2$, and $\mathrm{d}r=g$. Eq. (8) then yields

$$\delta E = \frac{B_0(z)^2\, g_0(z)^2\, u_0(z)}{2\mu_0 g(x,y,z,t,\varphi)}\,\mathrm{d}z\,\mathrm{d}\varphi. \tag{11}$$

According to Eq. (10), the force $\mathrm{d}f$ is given by

$$\mathrm{d}f = -\frac{\mathrm{d}}{\mathrm{d}g}(\delta E) = \frac{B_0(z)^2 g_0(z)^2 u_0(z)}{2\mu_0 g(x,y,z,t,\varphi)^2}\,\mathrm{d}z\,\mathrm{d}\varphi. \tag{12}$$

Hence, the total forces in the x- and y-directions can be expressed as

$$f_x = \frac{1}{2\mu_0}\int_0^{2\pi}\int_0^{l_0} \frac{B_0(z)^2 g_0(z)^2 u_0(z)}{g(x,y,z,t,\varphi)^2}\cos\varphi\,\mathrm{d}z\,\mathrm{d}\varphi, \tag{13}$$

$$f_y = \frac{1}{2\mu_0}\int_0^{2\pi}\int_0^{l_0} \frac{B_0(z)^2 g_0(z)^2 u_0(z)}{g(x,y,z,t,\varphi)^2}\sin\varphi\,\mathrm{d}z\,\mathrm{d}\varphi. \tag{14}$$

Table 1
Numerical values from the 18 MW hydropower generator

s_0	Average stator radius	2.775 m
l_0	Length of the generator	1.18 m
g_0	Average air-gap	0.0125 m
γ	Mass of the rotor	98165 kg
k	Stiffness of the axis	3.456×10^8 N/m
ω	Rotor rotation speed	14.2 rad/s
k_m	Magnetic stiffness	1.4715×10^8 N/m
μ_0	Permeability of air	$4\pi \times 10^{-7}$ Vs/Am

3.2. Properties of the UMP

The generator geometry and the B-field are now assumed constant in z through the generator length l_0. Numerical values from an 18 MW hydropower generator are used. The values are given in Table 1. These values are used in all simulations presented in this paper.

Fig. 4 shows UMP for the static case $x = y = 0$ with phase angles chosen to zero. Fig. 4(a) illustrates f_x and f_y for rotor and stator eccentricity, Fig. 4(b) shows f_x for stator eccentricity together with $\delta_n^r = 0.1g_0$, $n = 1, 2, 3$. Fig. 4(c) illustrates f_x and f_y for $\delta_2^r = \delta_3^s = 0.3g_0$, and Fig. 4(d) shows f_x for $\delta_2^r = \delta_m^s = 0.3g_0$, $m = 1, \ldots, 7$. Note that m even gives no UMP.

For ideal circular generator geometry and $y = 0$, the integral in Eq. (13) can be solved analytically to yield

$$f_x = \frac{l_0 g_0^2 B_0^2 u_0}{2\mu_0} \int_0^{2\pi} \frac{\cos\varphi}{(g_0 - x\cos\varphi)^2}\,\mathrm{d}\varphi = k_m \frac{x}{(1-(x^2/g_0^2)^{3/2}}. \tag{15}$$

Here, the magnetic stiffness, k_m, given in Table 1, is defined as

$$k_m = \frac{\pi l_0 B_0^2 u_0}{\mu_0 g_0}. \tag{16}$$

Eq. (15) is similar to results obtained by Wang et al. [14] and Sandarangani [19]. For $x \leqslant 0.1g_0$, the relative error is less than 2% when approximating Eq. (15) with the linear function $f^L = k_m x$. Therefore, a linear model of the UMP is interesting for small shape deviations and will be considered in Section 5.1.

4. The equation of motion

The equation of motion for the forced Jeffcott rotor is non-autonomous and nonlinear and consists of two second-order differential equations

$$\begin{aligned} \gamma\ddot{x} + c\dot{x} + kx &= f_x(x, y, t), \\ \gamma\ddot{y} + c\dot{y} + ky &= f_y(x, y, t). \end{aligned} \tag{17}$$

Here, γ is the mass of the rotor, k is the stiffness of the rotor axis and c being a linear viscous damping. In the case of the linear UMP, discussed in Section 5.1, the damped natural frequency becomes

$$\omega_d = \sqrt{\frac{k - k_m}{\gamma} - \left(\frac{c}{2\gamma}\right)^2} \approx 44.6\,\text{rad/s}. \tag{18}$$

The numerical values of k, k_m and γ can be found in Table 1. c is chosen to give the damping ratio $\zeta = 0.1$. The angular velocity, ω, of the rotor is 14.2 rad/s through all simulations. In non-dimensional form, Eqs. (17) yields

$$\begin{aligned} X'' + 2\zeta X' + X &= F_X(X, Y, \tau), \\ Y'' + 2\zeta Y' + Y &= F_Y(X, Y, \tau). \end{aligned} \tag{19}$$

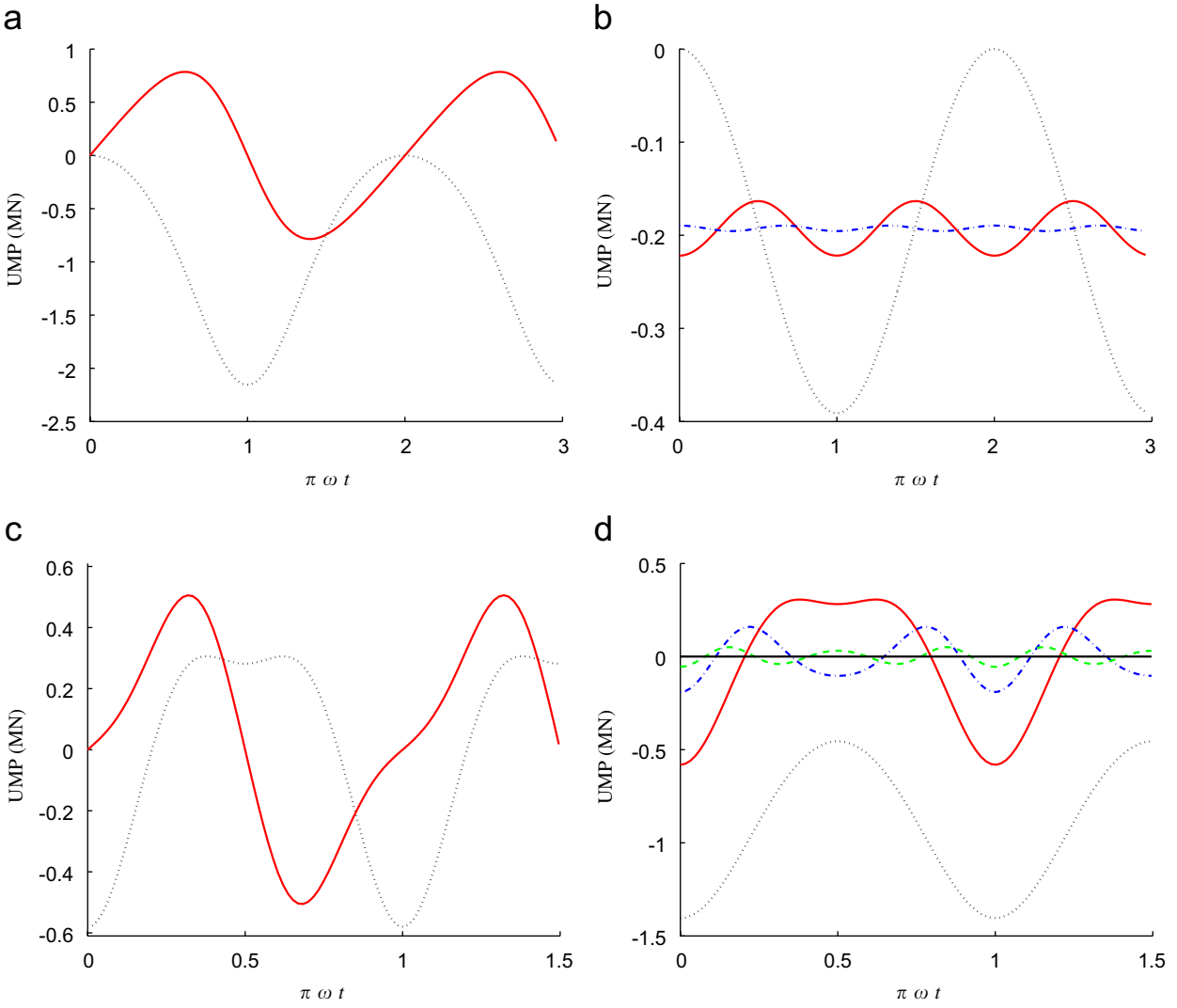

Fig. 4. UMP as a function of time t: (a) f_x (dotted) and f_y (solid), $\delta_1^s = \delta_1^r = 0.3g_0$; (b) f_x for $\delta_1^s = \delta_n^r = 0.1\,g_0$, $n = 1$ (dotted), $n = 2$ (solid), $n = 3$ (dashdot); (c) f_x (dotted) and f_y (solid), $\delta_2^r = \delta_3^s = 0.3\,g_0$; (d) f_x for $\delta_2^r = \delta_m^s = 0.3\,g_0$, $m = 1$ (dotted), $m = 2$ (solid), $m = 3$ (dashdot), $m = 4$ (dashed), m even (solid line at zero UMP).

Here, the non-dimensional quantities

$$X = \frac{x}{g_0}, \quad Y = \frac{y}{g_0}, \quad \Delta_n^R = \frac{\delta_n^r}{g_0}, \quad \Delta_m^S = \frac{\delta_m^S}{g_0}, \tag{20}$$

$$G = \frac{g(x, y, t, \varphi)}{g_0}, \quad \Omega = \omega\sqrt{\frac{\gamma}{k}}, \quad \tau = t\sqrt{\frac{k}{\gamma}}. \tag{21}$$

have been introduced. The notation implies differentiation with respect to the non-dimensional time τ. The air-gap G, and the forces F_X and F_Y yield

$$F_X = \frac{k_m}{2\pi k}\int_0^{2\pi} \frac{\cos\varphi}{G(X, Y, \tau, \varphi)^2}\,\mathrm{d}\varphi, \tag{22}$$

$$F_Y = \frac{k_m}{2\pi k}\int_0^{2\pi} \frac{\sin\,\varphi}{G(X,Y,\tau,\varphi)^2}\,\mathrm{d}\varphi, \tag{23}$$

$$G = 1 + \sum_{m=1}^{\infty} \Delta_m^S \cos\, m(\varphi + \alpha_m^s) - \sum_{n=1}^{\infty} \Delta_n^R \cos\, n(\varphi + \alpha_n^r - \Omega\tau) - X\cos\,\varphi - Y\sin\,\varphi. \tag{24}$$

5. Analysis

5.1. Linear model of the UMP

Recall from Section 3.2 that the UMP is nearly linear for small shape deviations. A linearization of Eqs. (22) and (23) can be obtained using the Maclaurin series

$$\frac{1}{(1-\varepsilon)^2} \approx 1 + 2\varepsilon, \tag{25}$$

with

$$\varepsilon = -\sum_{m=1}^{\infty} \Delta_m^S \cos\, m(\varphi + \alpha_m^s) + \sum_{n=1}^{\infty} \Delta_n^R \cos\, n(\varphi + \alpha_n^r - \Omega\,\tau) + X\cos\,\varphi + Y\sin\,\varphi. \tag{26}$$

From Eqs. (22) and (25), the linearization of F_X (F_X^L), can be expressed as

$$F_X^L = \frac{k_m}{2\pi k}\int_0^{2\pi} (1+2\varepsilon)\cos\,\varphi\,\mathrm{d}\varphi$$

$$= \frac{k_m}{k}(X - \Delta_1^S\cos\,\alpha_1^s + \Delta_1^R\cos(\Omega\tau - \alpha_1^r)). \tag{27}$$

Applying the same procedure in the Y-direction gives

$$F_Y^L = \frac{k_m}{k}(Y + \Delta_1^S\sin\,\alpha_1^s + \Delta_1^R\sin(\Omega\,\tau - \alpha_1^r)). \tag{28}$$

From Eqs. (27) and (28) it is clear that only Δ_1^R and Δ_1^S (rotor and stator eccentricity), affect the UMP.

5.2. Rotor or stator eccentricity

For ideal circular generator geometry, a stable equilibrium in the centre and a circle of unstable equilibria due to the nonlinear UMP exist in Eqs. (19). If stator eccentricity is added to this, i.e. $\Delta_1^S > 0$, these equilibria will move, and for a certain value of Δ_1^S stability is lost. If rotor eccentricity is added instead, i.e. $\Delta_1^R > 0$, there exists a circular limit cycle having periodicity equal to the driving frequency (synchronous whirling motion). Note that these kind of machines are always operating at undercritical conditions, recall Eq. (18). Therefore, when writing Eqs. (19) in polar coordinates

$$\begin{aligned} X &= R\cos\,\Theta, \\ Y &= R\sin\,\Theta, \end{aligned} \tag{29}$$

it is assumed that

$$R' = 0, \quad \text{and} \quad \Theta' = \begin{cases} \Omega, & \text{if } \Delta_1^R > 0, \\ 0, & \text{if } \Delta_1^S > 0. \end{cases} \tag{30}$$

With Eqs. (29) and (30), Eqs. (19) takes the form

$$\begin{aligned} &-R\Theta'^2\cos\Theta - 2\zeta R\Theta'\sin\Theta + R\cos\Theta = F_X,\\ &-R\Theta'^2\sin\Theta + 2\zeta R\Theta'\cos\Theta + R\sin\Theta = F_Y. \end{aligned} \tag{31}$$

With $F_R = F_X\cos\Theta + F_Y\sin\Theta$, this simplifies to

$$R(1-\Theta'^2) = F_R. \tag{32}$$

The term $R\Theta'^2$ corresponds to the centrifugal force. There is symmetry in the air-gap for both cases of eccentricity, and F_R will point towards the shortest air-gap. Therefore, F_R can be solved similar to Eq. (15), and the equation to solve yields

$$R(1-\Theta'^2) = \frac{k_m}{k}\frac{R+\Delta}{(1-(R+\Delta)^2)^{\frac{3}{2}}}, \quad \Delta = \begin{cases} \Delta_1^R, & \text{if } \Delta_1^R > 0,\\ -\Delta_1^S, & \text{if } \Delta_1^S > 0. \end{cases} \tag{33}$$

Thus, to use Eq. (33), Δ should be replaced by $-\Delta_1^S$ if stator eccentricity is considered, and by Δ_1^R if rotor eccentricity is considered. For zero eccentricity and the values given in Table 1, Eq. (33) has the solutions

$$R = 0 \quad \text{or} \quad R = \pm\sqrt{1-\left(\frac{k_m}{k(1-\Theta'^2)}\right)^{\frac{2}{3}}} \approx \begin{cases} \pm 0.6414 & \text{if } \Delta_1^R > 0,\\ \pm 0.6588 & \text{if } \Delta_1^S > 0. \end{cases} \tag{34}$$

By varying the eccentricity in Eq. (33), bifurcation diagrams relating to Eqs. (19) can be found numerically. The phase angle Θ_0 is introduced to give the direction of R, such that the negative solutions in R can be illustrated as positive with $\Theta_0 = \pi$. The bifurcation diagram for rotor eccentricity is shown in Fig. 5(a) and yields three limit cycles; C_1, C_2 and C_3. C_1 meets C_2 at $\Delta_1^R \approx 0.1658$, only C_1 is stable and is therefore of engineering interest. C_1 is the resulting attractor corresponding to synchronous whirling motion. C_3 corresponds to the phase $\Theta_0 = \pi$ whereas C_1 and C_2 to $\Theta_0 = 0$. This means that C_2 is the solution corresponding to the case when the rotor is moved in the same direction as C_1, and C_3 is the solution when the rotor is moved in the direction opposite to C_1. Thus, C_3 will exist for increasing Δ_1^R until the rotor hits the stator. The bifurcation diagram for stator eccentricity is shown in Fig. 5(b) and yields three equilibria; E_1, E_2 and E_3. E_1 meets E_2 in a fold-bifurcation at $\Delta_1^S \approx 0.1810$, only E_1 is stable and is therefore of engineering interest. E_3 corresponds to phase $\Theta = 0$ whereas E_1 and E_2 to $\Theta = \pi$. This means that E_2 is the solution

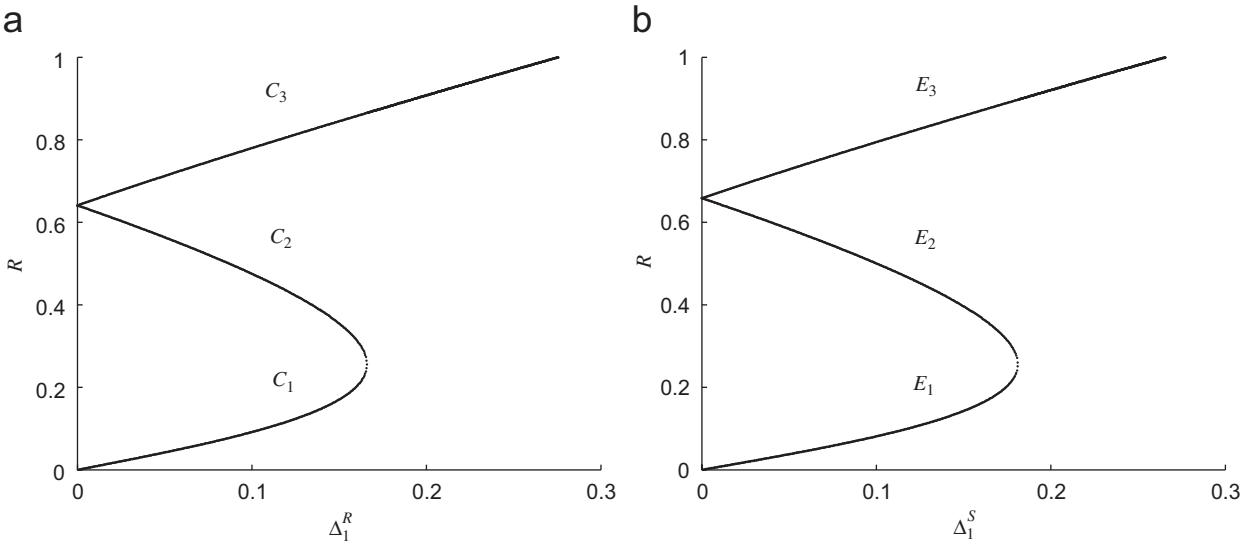

Fig. 5. Bifurcation diagrams to System (19): (a) $\Delta_1^R > 0$ (rotor eccentricity). R is the radius of limit cycles. (b) $\Delta_1^S > 0$ (stator eccentricity). R gives the location of equilibria.

corresponding to the case when the rotor is moved in the same direction as E_1, and E_3 is the solution when the rotor is moved in the direction opposite to E_1. Thus, E_3 will exist for increasing Δ_1^S until the rotor hits the stator. Note that it can exist also other attractors in these cases.

5.3. Stable equilibrium at the origin

When the rotor rotates at the origin, the UMP is zero for certain shape deviations due to their geometry, recall Fig. 2. The UMP is zero if G is periodic in φ with a period of $2\pi/q$, $q \in \mathbf{N}$ and $q \geqslant 2$. To see this, consider the UMP from each period of G. Since G is periodic and UMP is a function of only G, all q UMPs are identical. Therefore, the sum of the forces becomes zero if G passes two or more periods during one revolution. In these cases, only a moment in the z-direction can be induced by the electro-magnetic field. Fig. 6 shows the generator for the two simple cases $\Delta_2^R > 0, \Delta_2^S > 0$ (to the left) and $\Delta_2^R > 0, \Delta_3^S > 0$ (to the right). In the case $\Delta_2^R > 0, \Delta_2^S > 0$, G is periodic with period π and, therefore, the UMP is zero. This can be clarified by drawing a line through the origin with an arbitrary slope (dashed line in the figure). In the case $\Delta_2^R > 0, \Delta_3^S > 0$ the period of G is 2π and there will be a resulting UMP.

Thus, if it is possible to find an integer $q \geqslant 2$ such that

$$G(0,0,\tau,\varphi) = G\left(0,0,\tau,\varphi+\frac{2\pi}{q}\right) \tag{35}$$

holds, the UMP is zero. Here, G is given by Eq. (24) with $X = Y = 0$. Since Eq. (35) needs to hold $\forall \Delta_n^R \geqslant 0, \forall \Delta_m^S \geqslant 0, n, m \in \mathbf{N}$, and $\forall \tau \geqslant 0$, it reduces to

$$\cos n(\varphi + \alpha_n^r - \Omega\tau) = \cos n\left(\varphi + \alpha_n^r - \Omega\tau + \frac{2\pi}{q}\right) \quad \forall n \in \mathbf{N}^R, \tag{36}$$

$$\cos m(\varphi + \alpha_m^s) = \cos m\left(\varphi + \alpha_m^s + \frac{2\pi}{q}\right) \quad \forall m \in \mathbf{N}^S. \tag{37}$$

Here, $\mathbf{N}^R$ is the set of all natural numbers such that $\Delta_n^R > 0$, and $\mathbf{N}^S$ is the set of all natural numbers such that $\Delta_m^S > 0$. From Eqs. (36) and (37); if $\mathbf{N}^R$ is empty, Eq. (35) holds for $m \geqslant 2$; if $\mathbf{N}^S$ is empty, Eq. (35) holds for $n \geqslant 2$. If both $\mathbf{N}^S$ and $\mathbf{N}^R$ are empty, Eq. (35) holds (ideal circular geometry). Otherwise, Eq. (35) holds if it is possible to find integers p_n and p_m such that

$$q = \frac{n}{p_n} = \frac{m}{p_m} \geqslant 2, \quad q \in \mathbf{N} \quad \forall n \in \mathbf{N}^R \quad \forall m \in \mathbf{N}^S. \tag{38}$$

From Fig. 4(d), recall that f_x is zero for m even, since $n = 2$.

If Eq. (38) holds, the UMP is zero, and therefore, Eqs. (19) have an equilibrium at the origin. For small shape deviations this equilibrium is stable.

Noting that Σ is introduced to simplify the notation according to

$$\Sigma = \sum_{m=1}^{\infty} \Delta_m^S + \sum_{n=1}^{\infty} \Delta_n^R < 1. \tag{39}$$

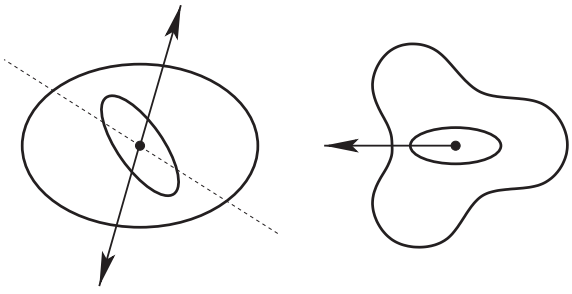

Fig. 6. The geometry of the generator for the two cases; $\Delta_2^R > 0, \Delta_2^S > 0$ (to the left) and $\Delta_2^R > 0, \Delta_3^S > 0$ (to the right).

It is proved (see Appendix A for the proof) that the equilibrium is stable if

$$\frac{2\pi+\sqrt{\pi^2+4}}{(1-\Sigma)^3}<\frac{2\pi k}{k_m}+\frac{\sqrt{\pi^2+4}}{(1+\Sigma)^3}. \tag{40}$$

Thus, if Eq. (38) is satisfied, Eqs. (19) have an equilibrium at the origin. This equilibrium is stable if Eq. (40) holds, and is for the specific machine considered in Table 1, if $\Sigma<0.16385$.

6. Simulated results

Note that the numerical values used in all simulations presented in this paper are taken from an existing 18 MW hydropower generator. These values are given in Table 1. Eqs. (19) is simulated using a fourth-order Runge–Kutta method. The force integrals given by Eqs. (22) and (23) are solved numerically at each step by Simpsons integrating method. For fixed parameters and different initial positions in the XY-plane, the trajectory is examined to see if it converges to an attractor without any impacts between the rotor and stator. The initial velocities are set to zero. With this method, an approximation is obtained of the two-dimensional XY-subspace of the basin of attraction to attractors without impacts between the rotor and stator. This approximation is denoted A_{XY}. The XY-plane is covered by a uniform grid of points. The simulation

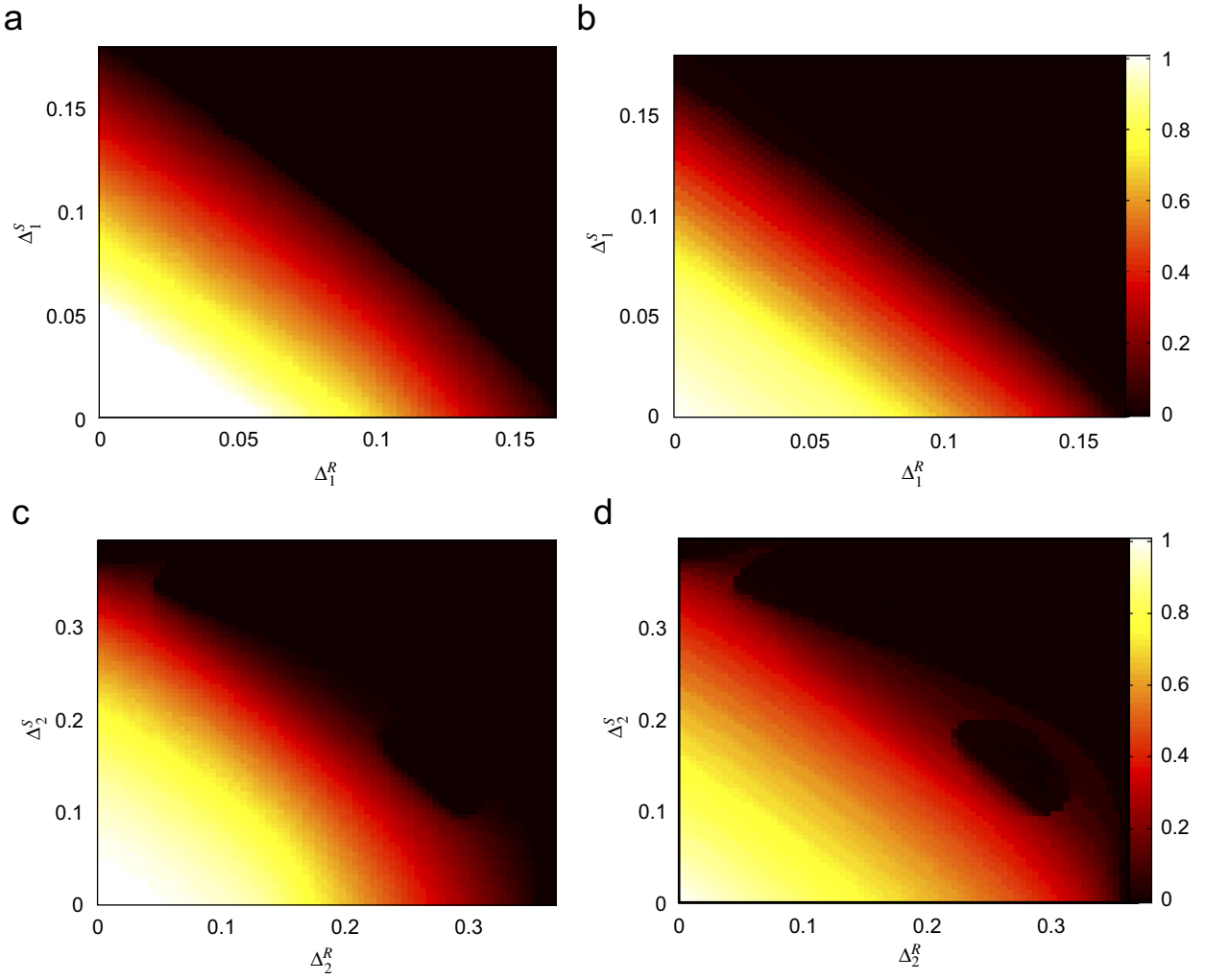

Fig. 7. (a) N_{XY} and (b) D_{XY} as a function of Δ_1^R, Δ_1^S (rotor and stator eccentricity). (c) N_{XY} and (d) D_{XY} as a function of Δ_2^R, Δ_2^S.

continues until the rotor hits the stator, comes close to an equilibrium, or reaches a time limit. The condition for reaching an equilibrium was set to $(X')^2 + (Y')^2 < 10^{-9}$. The time limit was set to 100 revolutions of the rotor. If the time limit or an equilibrium is attained, the corresponding initial position is said to be converging (otherwise diverging), and is added to A_{XY}. Since the shape of A_{XY} can be complicated, both the size and the shape of A_{XY} are considered. To measure the size, let n_{XY} be the number of elements in A_{XY}, and to measure the shape, let d_{XY} be the distance from the origin to the diverging point closest to the origin. This means that d_{XY} gives the radius of the largest circle, centred at the origin that is covered by A_{XY}. Then, to scale these measures, define

$$N_{XY} = \frac{n_{XY}}{n^0_{XY}}, \quad D_{XY} = \frac{d_{XY}}{d^0_{XY}}, \tag{41}$$

where n^0_{XY} and d^0_{XY} correspond to the case of ideal circular generator geometry. From Eq. (34), $d^0_{XY} = 0.6588$.

Figs. 7–9 show N_{XY} and D_{XY} as a function of different shape deviations. The uniform grid is chosen to give $n^0_{XY} = 1225$. The phase angles α^r_n and α^s_m are chosen due to symmetry. One simulation is needed for each phase angle combination. The values of n_{XY} and d_{XY} is taken as the worst case for each point in the $\Delta^R_n\,\Delta^S_m$-plane. Six phase angle combinations are considered in Figs. 7–9.

Fig. 10 also shows N_{XY} and D_{XY} as a function of different shape deviations, though as a function of one parameter at a time. The symmetry therefore allows the phase angles to be chosen to zero. The uniform grid is

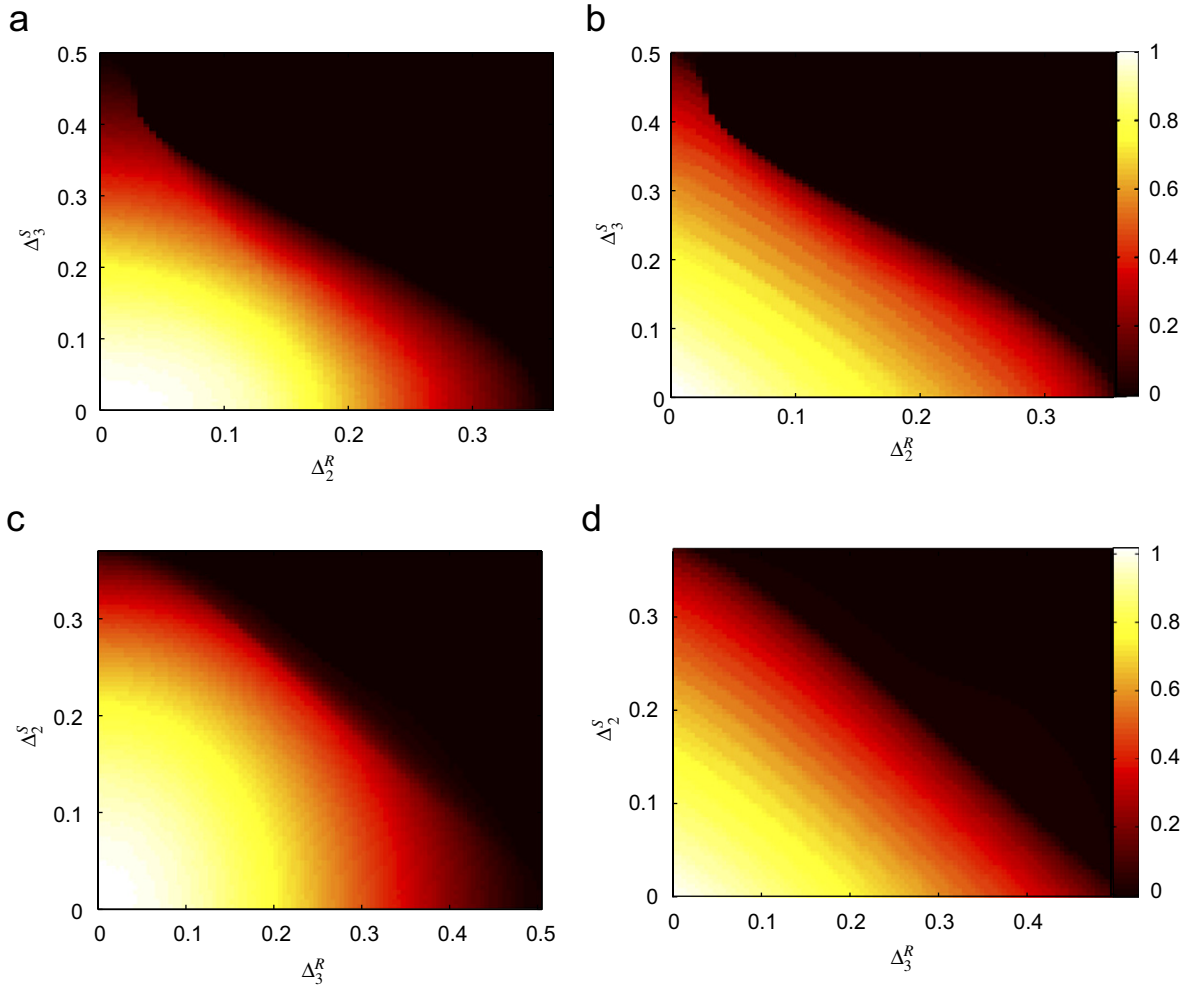

Fig. 8. (a) N_{XY} and (b) D_{XY} as a function of Δ^R_2, Δ^S_3. (c) N_{XY} and (d) D_{XY} as a function of Δ^R_3, Δ^S_2.

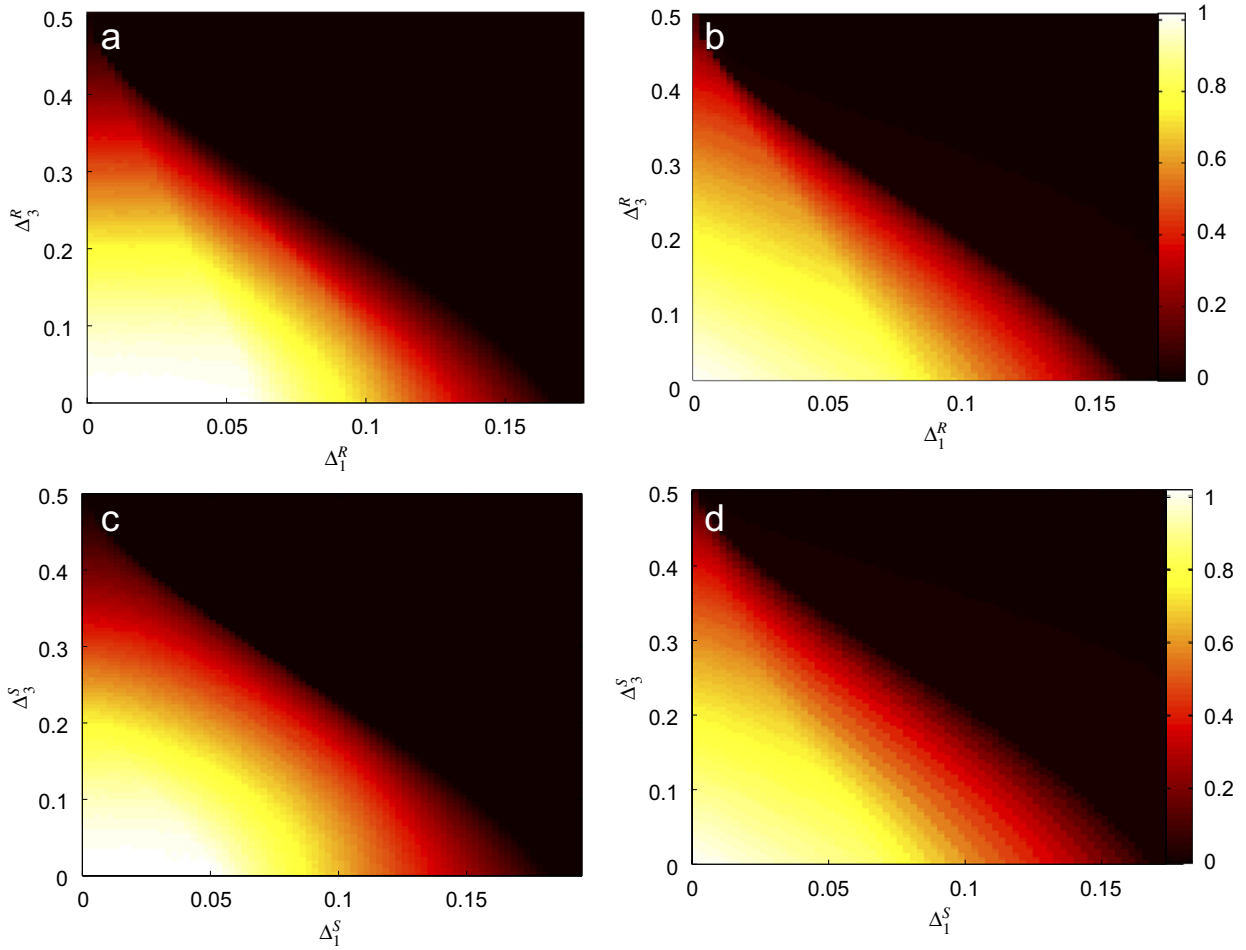

Fig. 9. (a) N_{XY} and (b) D_{XY} as a function of Δ_1^R, Δ_3^R. (c) N_{XY} and (d) D_{XY} as a function of and Δ_1^S, Δ_3^S.

refined to give $n_{XY}^0 = 13637$. Deviations of the rotor are considered in Fig. 10(a,b), and deviations of the stator in Fig. 10(c,d).

Figs. 11 and 12 shows A_{XY} and the corresponding attractor(s) for different shapes of the rotor and stator. In the figures the circle with radius $d_{XY}^0 = 0.6588$ is included to indicate the boundary of A_{XY} for the ideal circular generator. The phase angles are chosen to zero and the uniform grid is chosen to give $n_{XY}^0 = 13637$. In Figs. 7–10, the location of some of these illustrations can be found by using the values of Δ_n^R and Δ_m^S for each case. Deviations of the rotor are considered in Fig. 11(a–d), and deviations of the stator in Fig. 11(e–h). Fig. 12 shows some cases of Δ_m^S and Δ_n^R with and without Δ_1^S (stator eccentricity), and also two cases of very small A_{XY}.

7. Discussion and conclusions

In this paper, a mathematical model consisting of a Fourier series representation is developed to describe an arbitrary non-circular shape of the rotor and the stator. Since the length of these generators is relatively small, all parameters are considered constant in the z-direction for simplicity.

In Section 3.1, the UMP is derived through the law of energy conservation. The generator is treated as a continuum. This approximation can be made since the number of poles in hydropower generators are high (the generator considered in this paper has 44 poles). This method is used since it works for an arbitrary disturbed air-gap. Fig. 4 illustrates the complexity of the UMP even for simple shape deviations.

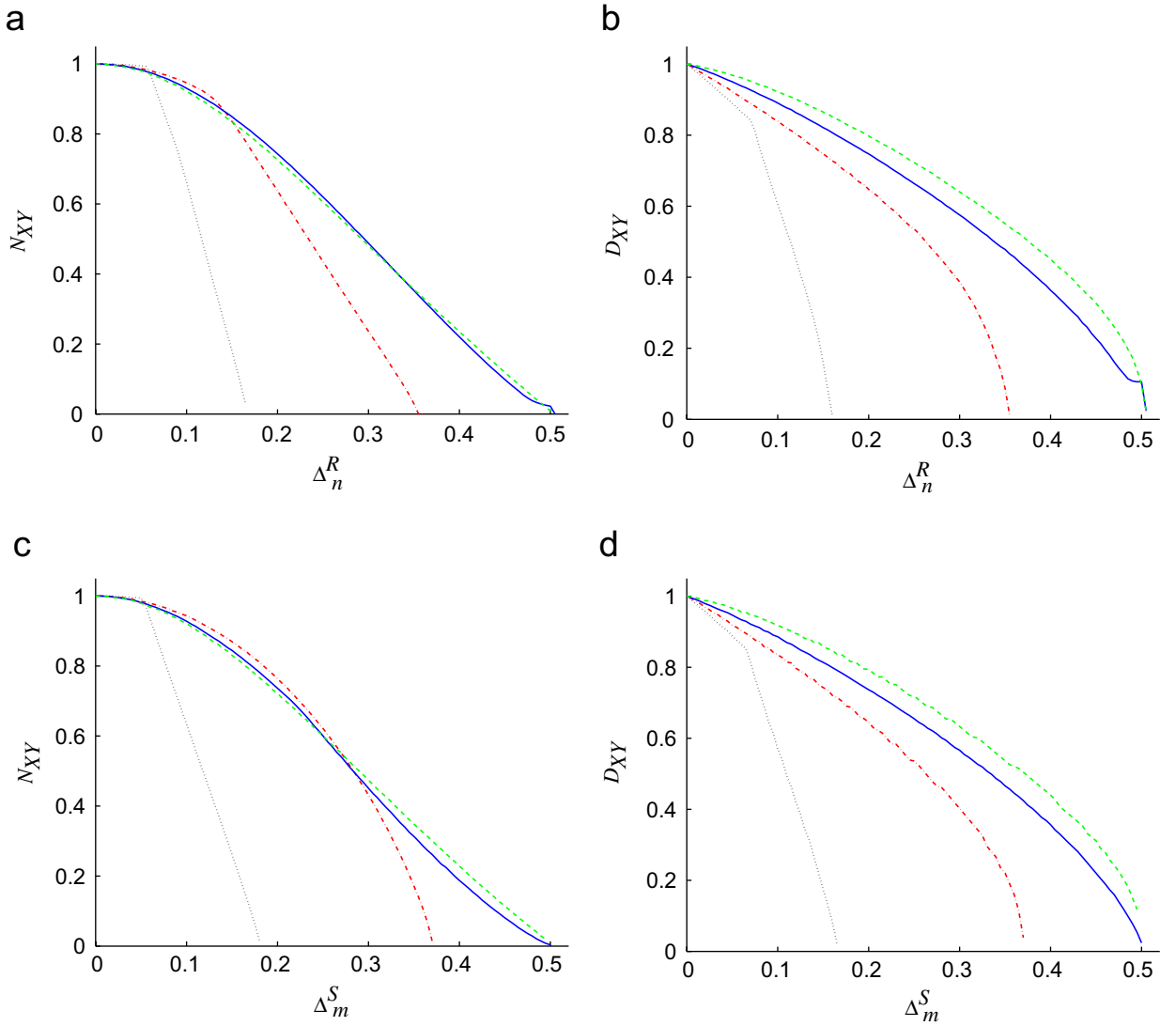

Fig. 10. (a) N_{XY} and (b) D_{XY} as a function of Δ_n^R, $n = 1$ (dotted), $n = 2$ (dashdot), $n = 3$ (solid) and $n = 4$ (dashed). (c) N_{XY} and (d) D_{XY} as a function of Δ_m^S, $m = 1$ (dotted), $m = 2$ (dashdot), $m = 3$ (solid) and $m = 4$ (dashed).

A linear model of the UMP is proposed in Section 5.1, since the nonlinear UMP derived in Section 3.1 has an almost linear behaviour for small eccentricities. When considering the linear model only Δ_1^R and Δ_1^S (rotor and stator eccentricity), affect the UMP and, therefore, the dynamics in the electric machine. Recall Eqs. (27) and (28). This result differs strongly from the nonlinear UMP, see Fig. 4(b), indicating the importance of considering the nonlinear effects. The results from Eqs. (27) and (28) can be understood by observing that the rotor/stator eccentricity is the only case where the deviation moves the geometrical centre of the rotor/stator, recall Fig. 2. Thus, there will be a constant force with stator eccentricity, and an oscillating force with rotor eccentricity.

In Section 5.2, the stability due to eccentricity is analysed. In the case of small stator eccentricity, one stable equilibrium exists. Following this equilibrium for increasing eccentricity, it is shown that the stability is lost in a fold bifurcation at $\Delta_1^S \approx 0.1810$. In the case of rotor eccentricity, a stable limit cycle exists. Following this cycle for increasing eccentricity, it is shown that the stability is lost at $\Delta_1^R \approx 0.1658$, See Fig. 5. This shows, when assuming that no other stable attractors exist, that the generator cannot operate without rotor–stator contact if rotor or stator eccentricity exceeds these values. The assumption above is strengthened by the simulations in Section 6. Fig. 7(a) agrees with these maximum values of eccentricity.

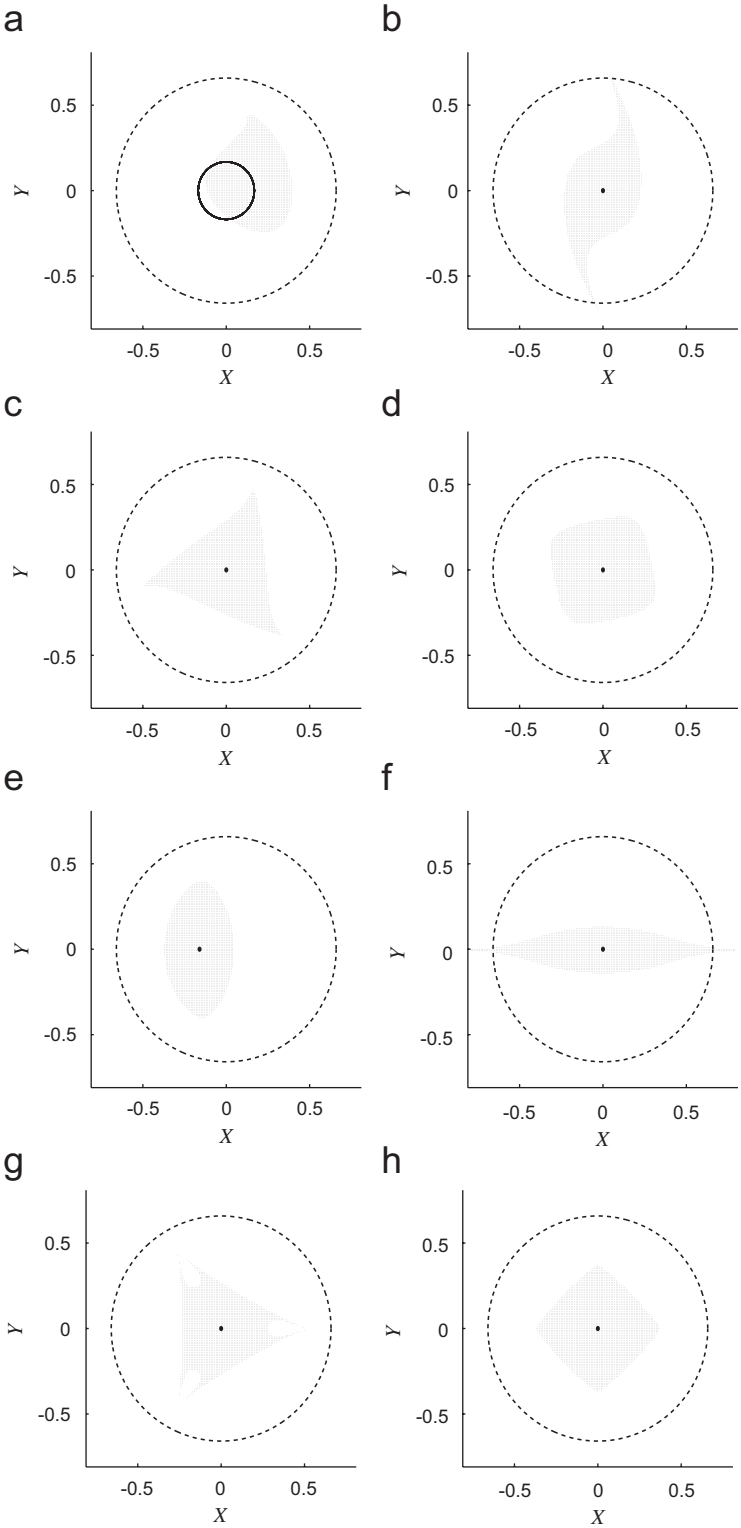

Fig. 11. A_{XY} and the corresponding attractor for some cases of $\Delta_n^R > 0$, and $\Delta_m^S > 0$ together with the boundary of A_{XY} for the ideal circular generator: (a) $\Delta_1^R = 0.15$; (b) $\Delta_2^R = 0.30$; (c) $\Delta_3^R = 0.40$; (d) $\Delta_4^R = 0.40$; (e) $\Delta_1^S = 0.16$; (f) $\Delta_2^S = 0.35$; (g) $\Delta_3^S = 0.40$; and (h) $\Delta_4^S = 0.40$.

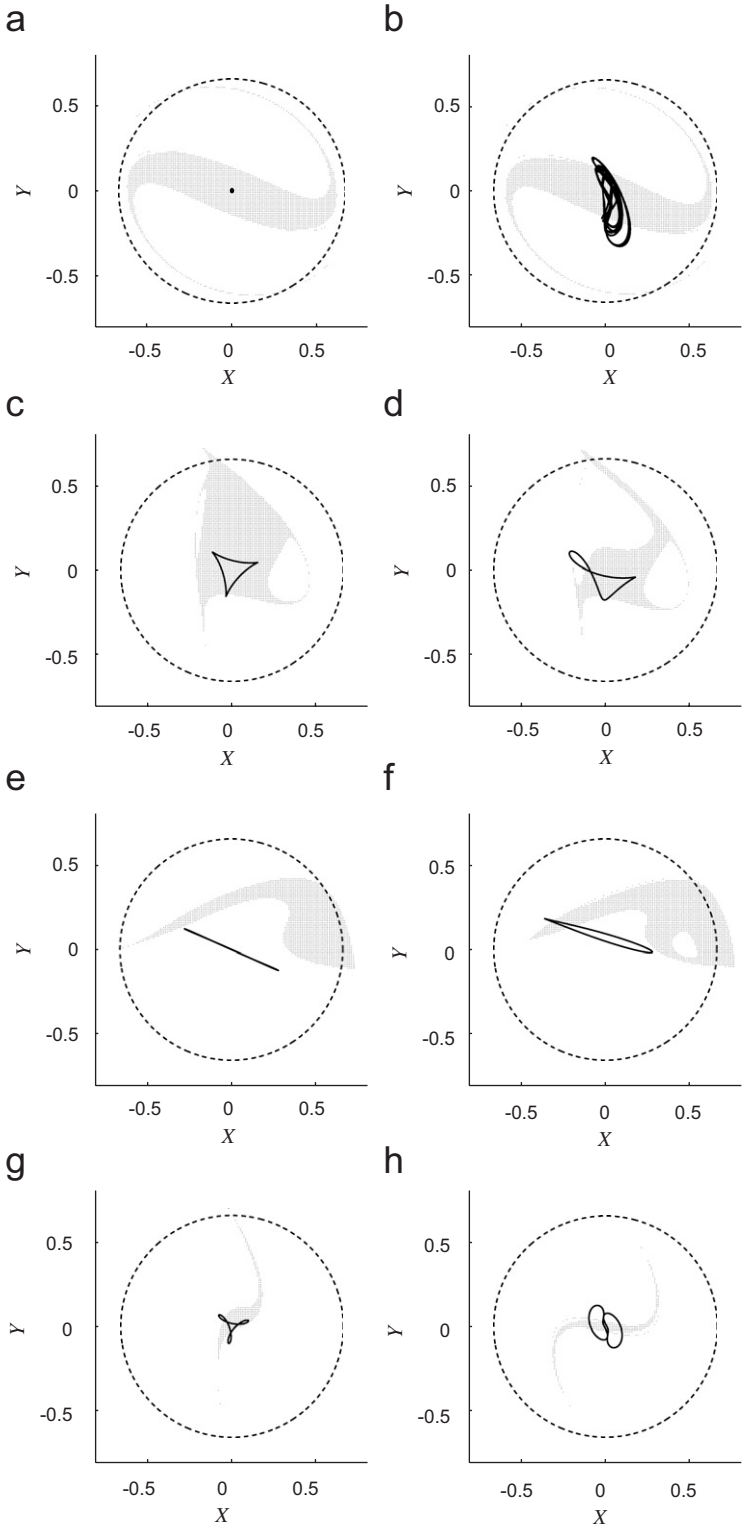

Fig. 12. A_{XY} and the corresponding attractor for some cases of shape deviations together with the boundary of A_{XY} for the ideal circular generator: (a) $\Delta_2^R = \Delta_2^S = 0.19$; (b) $\Delta_2^R = \Delta_2^S = 0.19$, $\Delta_1^S = 0.01$; (c) $\Delta_2^R = \Delta_3^S = 0.20$; (d) $\Delta_2^R = \Delta_3^S = 0.20$, $\Delta_1^S = 0.01$; (e) $\Delta_3^R = \Delta_2^S = 0.24$; (f) $\Delta_3^R = \Delta_2^S = 0.24$, $\Delta_1^S = 0.03$; (g) $\Delta_2^R = 0.33$, $\Delta_3^S = 0.08$; (h) $\Delta_2^R = 0.32$, $\Delta_2^S = 0.12$.

In Section 5.3, the UMP is proven to be zero for shape deviations according to Eq. (38), i.e. for these cases there exists an equilibrium at the origin. This result is general for electric machines if the UMP is assumed to be a function of only the air-gap width. It is proven that this equilibrium is stable if $\Sigma < 0.16385$ for the generator considered. Note that if all shape perturbation parameters are known for a machine, Σ can easily be calculated by adding these parameters according to Eq. (39). By assuming that this equilibrium is reached, this indicates that shape deviations satisfying Eq. (38) are preferable compared to other deviations for a generator. This assumption is strengthened by the simulations in Section 6, showing that in all tested cases, the trajectory reaches the origin.

Simulations of the basins of attraction are carried out in Section 6. From these simulations the importance of the shape deviations can be studied for the generator in question. To approximate the robustness of the safe solutions of a shape perturbed generator, both the size and the shape of A_{XY}, (recalling that this is the approximation of the two-dimensional XY-subspace of the basin of attraction) will be approximated. It is advantageous if A_{XY} is large and convex. (Recall that the measure of the size is N_{XY}, and the measure of the shape is D_{XY}, see Eq. (41) for the definitions). From Fig. 7(a) it is concluded that the effect of rotor and stator eccentricity, is nearly similar on N_{XY}. From Fig. 7(b) it can be seen that the same holds for D_{XY}. Hence, rotor and stator eccentricities affect the robustness in nearly the same way. Fig. 7(c,d) shows some differences between the rotor and stator for the case $\Delta_2^R > 0$, $\Delta_2^S > 0$, note some strange nonlinear effects near $\Delta_2^R = 0.25$, $\Delta_2^S = 0.15$. Fig. 8 illustrates some differences between the two cases $\Delta_2^R > 0$, $\Delta_3^S > 0$ and $\Delta_3^R > 0$, $\Delta_2^S > 0$. Note from Fig. 8(a,b) and Fig. 7(c,d) the strange behaviour for large stator perturbations and $0 < \Delta_2^R < 0.05$. Similarities between the rotor and stator are shown in Fig. 9, where the same shape deviations are considered for the rotor in Fig. 9(a,b) and for the stator in Fig. 9(c,d). Fig. 9(a,b) shows rotor eccentricity combined with $\Delta_3^R > 0$ whereas Fig. 9(c,d) shows stator eccentricity combined with $\Delta_3^S > 0$. Figs. 7–10 all illustrate that the effect of the shape deviations to N_{XY} and D_{XY} decreases when m and n increases. Thus, assuming the same amount of deviation, this shows that eccentricity, i.e. Δ_1^R and Δ_1^S, are more severe than deviations corresponding to higher m and n. Sharp knees are observed near $\Delta_1^R = 0.05$ and near $\Delta_1^S = 0.05$ in Fig. 10, meaning that deviations less than 5% of the air-gap of the generator only marginally affect the robustness. Moreover, it is of interest to discuss A_{XY}. Complicated A_{XY} occurs in some cases shown in Fig. 12. This illustrates the complexity of the dynamics; therefore, both N_{XY} and D_{XY} have to be considered for investigating how robust different shape deviations are in these cases. Simple periodic attractors occur in some cases, but more complicated attractors also exist. See Fig. 12(b–h). In Fig. 12(b) there are at least two attractors present, with very long period or chaotic behaviour, and in Fig. 12(h), there are two attractors present. This also indicates the existence of multiple solutions.

Note that $\omega = 14.2\,\mathrm{rad/s}$ was used in all simulations. Since ω is not close to ω_d, recall Eq. (18), and since rotor eccentricity will give synchronous whirling motion, the rotor is not close to resonance in the case of rotor eccentricity. Thus, the results presented in Section 6, showing that the cases of rotor eccentricity being the worst in the case of robustness, cannot be trivially explained by excitations of the damped natural frequency. This can also be understood by observing that stator eccentricity affects the robustness nearly similar to rotor eccentricity, and stator eccentricity gives only a stationary point.

Since UMP can cause large vibrations in hydropower generators which can destroy the machine, the shape of the rotor and stator is frequently measured during maintenance. The results from this paper can be used to evaluate such measurements and estimate the stability and robustness through simulations. When using the mathematical methods presented in this paper on a real machine, the unbalance and the dominating shape perturbation parameters has to be included. Then a simulation of the robustness can be carried out, where N_{XY} and D_{XY} will be found for the generator considered. Many results presented in this paper are general and can be applied to different electric motors and generators. This paper indicates which tolerances are more important than others when constructing new machines.

Acknowledgments

Elforsk AB and the Swedish Energy Authority by the Elektra research program are acknowledged for the financial support of this project.

Appendix A. Proof of Eq. (38)

The eigenvalues of the Jacobian matrix to Eqs. (19) at the origin yield,

$$\lambda_{1,2} = -\zeta + \sqrt{\zeta^2 + \alpha \pm \beta},$$
$$\lambda_{3,4} = -\zeta - \sqrt{\zeta^2 + \alpha \pm \beta}, \tag{A.1}$$

where

$$\alpha = \frac{1}{2}\left(\frac{\partial F_X}{\partial X} + \frac{\partial F_Y}{\partial Y}\right) - 1, \quad \beta = \frac{1}{2}\sqrt{\left(\frac{\partial F_X}{\partial X} - \frac{\partial F_Y}{\partial Y}\right)^2 + 4\,\frac{\partial F_X}{\partial Y}\,\frac{\partial F_Y}{\partial X}}. \tag{A.2}$$

All derivatives are hereinafter evaluated at the origin. Clearly $\mathrm{Re}\,\lambda_{3,4} < 0$. From Eqs. (22) and (23), it is concluded that

$$\frac{\partial F_X}{\partial Y} = \frac{\partial F_Y}{\partial X}. \tag{A.3}$$

Therefore, $\beta > 0$ and real, and it follows that $\mathrm{Re}\,\lambda_{1,2} < 0$ if and only if

$$\alpha + \beta < 0. \tag{A.4}$$

The derivatives of the force integrals have the following bounds:

$$L < \frac{\partial F_X}{\partial X} < U, \quad L < \frac{\partial F_Y}{\partial Y} < U \tag{A.5}$$

and

$$\left|\frac{\partial F_X}{\partial Y}\right| < \frac{1}{\pi}(U - L), \tag{A.6}$$

where

$$L = \frac{k_m}{k(1+\Sigma)^3} \quad \text{and} \quad U = \frac{k_m}{k(1-\Sigma)^3}. \tag{A.7}$$

Noting that Σ is introduced to simplify the notation. To prove Eqs. (A.5) and (A.6), observe from Eqs. (3) and (20) that

$$\Sigma = \sum_{m=1}^{\infty} \Delta_m^S + \sum_{n=1}^{\infty} \Delta_n^R < 1. \tag{A.8}$$

Further, since $\Delta_n^R > 0$ and $\Delta_m^S > 0$,

$$G(0,0,\tau,\varphi) = 1 + \sum_{m=1}^{\infty} \Delta_m^S \cos m(\varphi + \alpha_m^s) - \sum_{n=1}^{\infty} \Delta_n^R \cos n(\varphi + \alpha_n^r - \omega t)$$
$$\geqslant 1 - \Sigma. \tag{A.9}$$

With Eq. (A.9), the upper bound of $\partial F_X/\partial X$ yields

$$\begin{aligned}\frac{\partial F_X}{\partial X} &= \frac{k_m}{2\pi k}\int_0^{2\pi}\frac{\partial}{\partial X}\left(\frac{1}{G(0,0,\tau,\varphi)^2}\right)\cos\varphi\,\mathrm{d}\varphi \\ &= \frac{k_m}{k\pi}\int_0^{2\pi}\frac{\cos^2\varphi}{G(0,0,\tau,\varphi)^3}\,\mathrm{d}\varphi \\ &\leqslant \frac{k_m}{k\pi(1-\Sigma)^3}\int_0^{2\pi}\cos^2\varphi\,\mathrm{d}\varphi \\ &= \frac{k_m}{k(1-\Sigma)^3} = U. \end{aligned} \tag{A.10}$$

The proof of all inequalities in Eq. (A.5) is similar. To prove Eq. (A.6), consider the upper bound of $\partial F_X/\partial Y$, here $\kappa = k_m/(2\pi k)$ is introduced, and the arguments of G are omitted to save space,

$$\begin{aligned}\frac{\partial F_X}{\partial Y} &= \frac{k_m}{2\pi k}\int_0^{2\pi}\frac{\sin 2\varphi}{G(0,0,\tau,\varphi)^3}\,\mathrm{d}\varphi \\ &= \kappa\left(\int_0^{\pi/2}\frac{\sin 2\varphi}{G^3}\,\mathrm{d}\varphi + \int_{\pi/2}^{\pi}\frac{\sin 2\varphi}{G^3}\,\mathrm{d}\varphi + \int_{\pi}^{3\pi/2}\frac{\sin 2\varphi}{G^3}\,\mathrm{d}\varphi + \int_{3\pi/2}^{2\pi}\frac{\sin 2\varphi}{G^3}\,\mathrm{d}\varphi\right) \\ &\leqslant \kappa\left(\frac{\int_0^{\pi/2}\sin 2\varphi}{(1-\Sigma)^3}\,\mathrm{d}\varphi + \frac{\int_{\pi/2}^{\pi}\sin 2\varphi}{(1+\Sigma)^3}\,\mathrm{d}\varphi + \frac{\int_{\pi}^{3\pi/2}\sin 2\varphi}{(1-\Sigma)^3}\,\mathrm{d}\varphi + \frac{\int_{3\pi/2}^{2\pi}\sin 2\varphi}{(1+\Sigma)^3}\,\mathrm{d}\varphi\right) \\ &= \frac{k_m}{k\pi}\left(\frac{1}{(1-\Sigma)^3} - \frac{1}{(1+\Sigma)^3}\right) = \frac{1}{\pi}(U-L). \end{aligned} \tag{A.11}$$

The proof of the lower bound in Eq. (A.6) is similar. With Eqs. (A.5), (A.6) and (A.7), Eq. (A.4) holds true if

$$\alpha+\beta < U - 1 + \frac{1}{2}\sqrt{(U-L)^2 + \frac{1}{\pi^2}(U-L)^2} < 0. \tag{A.12}$$

This simplifies to

$$\frac{2\pi+\sqrt{\pi^2+4}}{(1-\Sigma)^3} < \frac{2\pi k}{k_m} + \frac{\sqrt{\pi^2+4}}{(1+\Sigma)^3}, \tag{A.13}$$

and the proof is complete.

References

[1] P. Talas, P. Toom, Dynamic measurement and analysis of air-gap variations in large hydroelectric generators, *IEEE* 83 WM 226-8 (1983) 9.
[2] B.A. Behrend, On the mechanical force in dynamos caused by magnetic attraction, *AIEE* 17 (1900) 617.
[3] R.C. Robinson, The calculation of unbalanced magnetic pull in synchronous and induction motors, *Electrical Engineering* 62 (1943) 620–624.
[4] A. Covo, Unbalanced magnetic pull in induction motors with eccentric rotors, *Transactions of the AIEE* 73 (Part 3) (1954) 1421–1425.
[5] H. Ohishi, S. Sakabe, K. Tsumagari, K. Yamashita, Radial magnetic pull in salient poles machines with eccentric rotors, *IEEE* 86 SM 475-8 (1986) 5.
[6] R. Belmans , W. Geysen, H. Jordan, A. Vandenput, Unbalanced magnetic pull in three phase two pole induction motors with eccentric rotors, *IEE Conference Publication* No. 213, 1982, pp. 65–69.

[7] J. Fruchtenicht, H. Jordan, H.O. Seinsch, Running instability of cage induction motors caused by harmonic fields due to eccentricity. Part 1: Electro-Magnetic Spring Constant and Electro-Magnetic Damping Coefficient. Part 2: Self-Exited Transverse Vibrations of the Rotor, *Archiv fur Elektrotechnik* 65(4–5) (1982) 271–292.
[8] R. Belmans, A. Vandenput, W. Geysen, Influence of unbalanced magnetic pull on the radial stability of flexible-shaft induction machines, *IEE Proceedings, Part B: Electric Power Applications* 134 (2) (1987) 101–109.
[9] A.C. Smith, D.G. Dorrell, Calculation and measurement of unbalanced magnetic pull in cage induction motors with eccentric rotors. Part 1: Analytical Model, *IEE Proceedings Electric Power Applications* 143 (3) (1996) 193–201.
[10] M.J. Debortoli, S.J. Salon, D.W. Burrow, C.J. Slavik, Effect of rotor eccentricity and parallel windings on induction machine behaviour: A study using finite element analysis, *IEEE Transaction on Magnetics* 29 (1993) 1676–1682.
[11] A. Arkkio, Unbalanced magnetic pull in cage induction motors with asymmetry in rotor structures, *Eighth International Conference on Electrical Machines and Drives*, 1–3 September, Conference Publication No. 444, Cambridge, 1997.
[12] D.G. Dorrell, Modelling of non-uniform rotor eccentricity and calculation of unbalanced magnetic pull in 3-phase cage induction motors, ICEM, Espoo, Finland, 28–30 August, 2000.
[13] D. Guo, F. Chu, D. Chen, The unbalanced magnetic pull and its effects on vibration in a three-phase generator with eccentric rotor, *Journal of Sound and Vibration* 254 (2) (2002) 297–312.
[14] Y. Wang, G. Sun, L. Huang, Magnetic field-induced nonlinear vibration of an unbalanced rotor, ASME, Design Engineering Division (Publication) DE, Vol. 116(2); *Proceedings of the ASME Design Engineering Division*, Vol. 2, 2003, pp. 925–930.
[15] T.P. Holopainen, A. Tenhunen, A. Arkkio, Electromechanical interaction in rotordynamics of cage induction motors, *Journal of Sound and Vibration*, 284(3–5) June 21, 2005, pp. 733–755.
[16] M. Karlsson, Jan-Olov Aidanpää, Dynamic behaviour in a hydro power rotor system due to the influence of generator shape and fluid dynamics, *ASME Power*, Chicago, IL, April 5–7, 2005, pp. 905–913.
[17] S. Williamson, M.A.S. Abdel-Magied, Unbalanced magnetic pull in induction motors with asymmetrical rotor cages, *IEE Conference Publication*, No. 254, 1985, pp. 218–222.
[18] R.K. Wangsness, Electromagnetic fields, Hamilton Printing Company, 1986, ISBN 0-471-81186-6.
[19] C. Sandarangani, Electrical machines design and analysis of induction and permanent magnet motors, Royal Institute of Technology, Stockholm, 2000.